Stable and high current emission of electrons from a HfC nanoneedle field-emitter fabricated by focused-ion beam

Shuai Tang[1†], Jie Tang[1,2*], Yimeng Wu[1,2], You-Hu Chen[1], Jun Uzuhashi[1], Tadakatsu Ohkubo[1], Masaki Takeguchi[1], Lu-Chang Qin[3*]

[1]National Institute for Materials Science, Tsukuba, Ibaraki 305-0047, Japan

[2]Graduate School of Pure and Applied Science, University of Tsukuba, Tsukuba, Ibaraki 305-8857, Japan

[3]Department of Physics and Astronomy, University of North Carolina at Chapel Hill, Chapel Hill, NC 27599-3255, USA

[†]Present address: State Key Lab of Optoelectronic Materials and Technologies, Guangdong Province Key Laboratory of Display Material and Technology, School of Electronics and Information Technology, Sun Yat-sen University, Guangzhou 510275, China

Corresponding email: tang.jie@nims.go.jp, lcqin@email.unc.edu

Abstract

HfC nanoneedle with both excellent electron emission characteristics and robust structure is regarded as a potential candidate for field-emission point electron source especially high emission current. Herewith, the HfC nanoneedle emitter has been fabricated by focused ion beam method. The transmission electron microscope with energy dispersive spectrum characterization show it has a sharp tip of curvature of radius of 10-20 nm and the structure is single crystalline with <100> orientation. The HfC nanoneedle emitter shows a convergent beam, low work function of 3.2 eV and also low turn-on field and threshold field of 2.7 V/nm and 3.5 V/nm at 2 nA and 50 nA respectively. It also shows a good field emission stability with fluctuation as 1.4%/30 mins and 1.5%/15 mins under normal (50 nA) and high current (280 nA) respectively.

Keywords: HfC nanoneedle, electron source, stable field emission, high current, focused-ion beam

Introduction

Cold field-emission (CFE) point electron source shows the highest brightness and smallest energy spread which is the best candidate for electron beam systems including imaging, inspection, and lithography [1-2]. However, the only viable tungsten CFE point electron source remains to have two major shortcomings: (i) it has a high work

function (~4.3 eV) which limits its energy spread and therefore the resolution in imaging system; (ii) it usually emits an unstable current with rapid decays [3-5]. During the past six decades, many materials including metal nanotips, carbon nanotube, graphene, and nanowires have been explored and studied for the application as field-emission point electron sources [6-22].

Hafnium carbide (HfC) has shown great potential for application as field-emission electron sources due to its high melting point, excellent thermal and electrical conductivities, low work function, outstanding mechanical strength, and especially high current emission capability [23-25]. The field-emission characteristics are usually determined not only by the chemical composition of the emitter material, but also by the morphology and structure of the emitter surface. To explore the optimal morphology and structure of nanostructures for field emission, several types of HfC structures have been investigated over the past 30 years. Started from 1990s, HfC tips have been fabricated by electrochemical polishing and their field emission performance has been measured and reported in several publications [18-20]. Kagarice et al. reported the field emission characteristics from (310)-oriented single-crystalline HfC tip with tip radius of 150-300 nm fabricated by electrochemical polishing and it showed a lower work function, higher emission brightness, lower energy spread, and more stable emission current than W(310) CFE point electron source [20]. However, the fluctuations of emission current were still greater than 10%/h in a high vacuum of 6×10^{-8} Pa, which was concluded as unsatisfactory for practical uses. HfC films or nanorods were also deposited on carbon nanotubes or silicon tips to improve the emission current and emission stability [26-28]. Recently, we began to utilize HfC nanowires that have a single-crystalline structure and also large aspect ratio beneficial for field emission performance [12-14]. The results showed high emission brightness, excellent emission stability, and narrow energy spread when the HfC nanowire was sharpened by using field-evaporation or focused ion beam (FIB) processing [13,14]. However, the inevitable mechanical vibrations of the suspended HfC nanowire structure and the

complex fabrication process still impose limitations on making it scalable in fabrication and process control.

Recently, we have developed a FIB method to enable controllable and efficient fabrication of CFE nanoneedle emitters that possess a sharp and crystalline tip with a robust structure [29-30]. Furthermore, the FIB-processed LaB_6 CFE nanoneedle emitter was installed in a TEM and showed the desired capabilities of atomic imaging with sub-angstrom resolution and especially long-term stability [31]. Therefore, the FIB method is now a technique of choice naturally to prepare HfC nanoneedle emitters to examine the electron emission characteristics of an HfC CFE point electron source.

In this work, an HfC nanoneedle field-emitter has been fabricated by the FIB method. The atomic structure and elemental distribution of the HfC nanoneedle field-emitter have been characterized by scanning transmission electron microscopy (STEM) with energy-dispersive X-ray spectroscopy (EDS). The field emission measurements showed that the HfC nanoneedle has a low work function of 3.2 eV and also a low turn-on field of 2.7 V/nm at an emission current of 2 nA. The characteristics of a single emission spot, excellent emission stability, and high emission current make the HfC an outstanding candidate for the CFE point electron source.

Results and discussion

The HfC nanoneedle emitter was fabricated from a single crystalline HfC bulk and attached onto a tungsten platform by a standard lift-out method using a FIB system [29-30]. Figure 1a is a typical bright-field TEM image of the HfC field-emission nanoneedle after FIB fabrication and it has a very sharp tip with a curvature of radius of ~10 nm. The inset in Figure 1a is a selected area electron diffraction (SAED) pattern of the tip apex of the HfC nanoneedle which shows that the nanoneedle is single crystalline and aligned in the <001> direction. Figure 1b is a high-resolution high-angle annular dark-field (HAADF-) STEM image of tip marked with blue box in Figure 1a. The single-crystalline structure of the nanoneedle is observed clearly. The spacings of 0.23 nm and

0.27 nm correspond to the {002} and {111} lattice planes of HfC, respectively. In addition, the HfC tip has a thin amorphous layer with a thickness of about 3 nm on the surface. To further reveal the surface structure of the HfC nanoneedle, the chemical composition was obtained by EDS mapping and the elemental distribution of Hf, C, and O is shown in Figure 1c-e, respectively. The distribution of Hf (Figure 1c) increased gradually from surface to interior while the distribution of C (Figure 1d) is nearly uniform throughout the nanoneedle. Oxygen is present due to surface oxidation and its distribution (Figure 1e) is concentrated at the surface only. Figure 1g is a line profile, drawn from the region indicated by the yellow arrow (Figure 1c), of the distributions of Hf, C, and O. It reveals that the concentration of Hf, C, O as a function of depth. The ratio of the elements Hf : C : O at the amorphous layer (depth of 3 nm) is 1.0:1.7:1.8 and at depth greater than 6 nm is 1.0:1.0:0.3, respectively, indicating that the interior is HfC and the amorphous layer on surface has a composite structure of Hf-C-O, which is induced by oxidation and carbon contamination during exposure to air. It should be noted that, before field emission measurement, thermal flashing was applied to remove the surface layer [32].

The field-emission characteristics of the HfC emitters were measured in a high vacuum chamber with base pressure of 1×10^{-7} Pa. Figure 2a is a scanning electron microscope (SEM) image of the HfC nanoneedle. It has a sharp tip with a radius of ~15 nm. Compared with the HfC nanowire emitter, the nanoneedle emitter has a much more robust structure, beneficial for both dissipation of heat due to emission of high electric current and relieving the vibrations in high electric field. The inset in Figure 2a is a field emission pattern. Due to its sharp tip, the HfC nanoneedle emitter has single emission spot which is important for obtaining a high brightness of electron emission. Figure 2b is the current-voltage (I-V) curve of the electron emission and Figure 2c is its corresponding Fowler-Nordheim (F-N) plot, respectively. The turn-on voltage is only 205 V when the emission current is set at 2 nA and the threshold voltage is 260 V when the emission current is set at 50 nA. The F-N plot shows excellent linearity with R^2-

factor of 0.996, confirming that it is cold-field emission indeed.

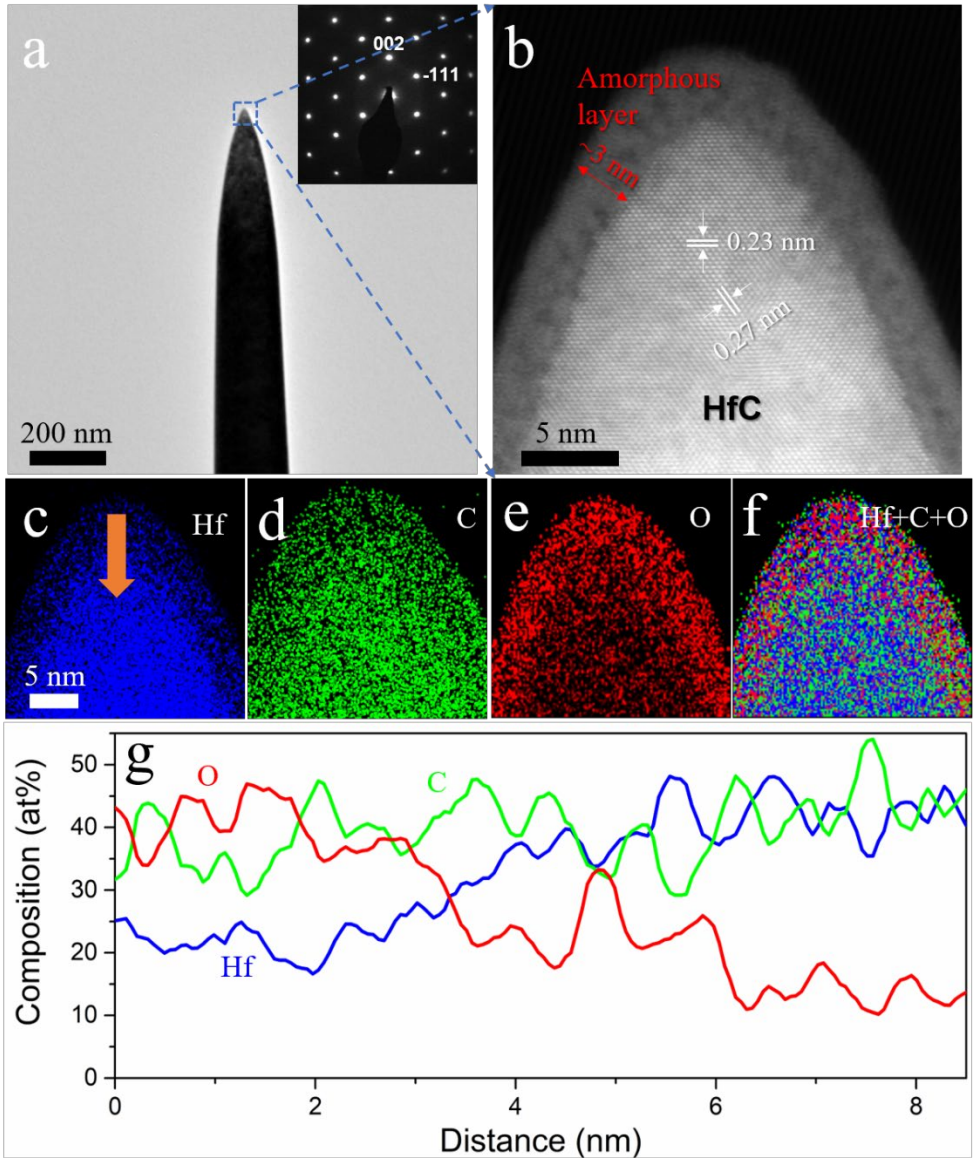

Figure 1 TEM characterization of HfC nanoneedle field-emiitter. (a) Typical TEM image with inset being SAED of the tip; (b) High-resolution HAADF-STEM image of HfC nanoneedle tip marked with blue box in (a); (c-f) EDS maps of HfC nanoneedle showing distribution of element (c) Hf, (d) C, (e) O, and (f) Hf+C+O; (g) Depth profile along the arrow indicated in (c) showing concentration of Hf (blue), C (green), and O (red).

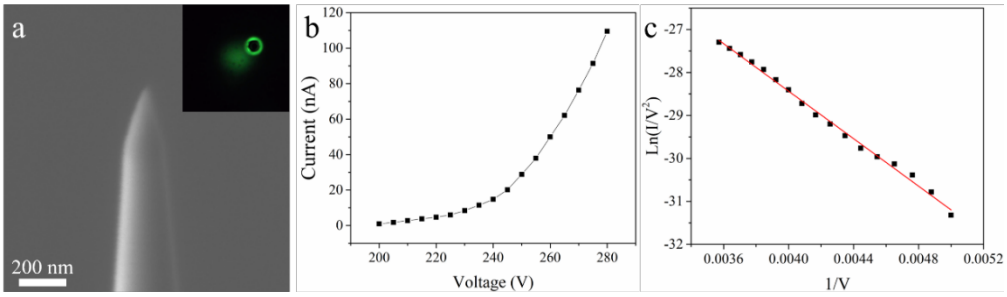

Figure 2 Measurement of field-emission characteristics. (a) SEM image of HfC nanoneedle with inset being the FEM pattern; (b-c) Field-emission I-V and corresponding F-N curves.

Herewith the improved F-N theory is invoked to analyse the field-emission data [33-36]. The field-emission current is given as

$$I = \frac{Ac_1F^2}{\phi}\exp\left(\frac{-V_F c_2 \phi^{\frac{3}{2}}}{F}\right) \tag{1}$$

where I is the emission current, A is the emission area, ϕ is the work function in eV, $c_1 = 1.54\times10^{-6}$ eV V^{-2}, $c_2 = 6.83\times10^{9}$ eV$^{-3/2}$ V m^{-1}, and F is the electric field at the tip apex of the emitter that can be expressed as

$$F = \beta V \tag{2}$$

in which $\boldsymbol{\beta}$ is a proportionality factor relating the extraction voltage V and the electric field F, and V_F is the appropriate particular value of a current correction function that is related to the work function ϕ and the relevant local surface field F. It is expressed as

$$\boldsymbol{V_F = v(y) = 1 - y^2 + \frac{1}{3}y^2 \ln(y)}\ , \tag{3}$$

in which $\boldsymbol{y = cF^{1/2}/\phi}$ and $c = 1.2$ eV V$^{-1/2}$ nm$^{1/2}$.

The linearized F-N plot of $ln(I/V^2)$ vs. $1/V$, *i.e.,*

$$\ln\left(\frac{I}{V^2}\right) = \frac{k}{V} + b\ , \tag{4}$$

has a slope $\boldsymbol{k = -s_t c_2 \phi^{3/2}/\beta}$ and intercept $\boldsymbol{b = \ln(Ac_1\beta^2 r/\phi)}$, where s_t and r are the appropriate value of a slope correction function and intercept correction function, respectively,

$$s(y) = 1 - \frac{1}{6}y^2 \tag{5}$$

and

$$r(y) = (1 + \frac{1}{9}[y^2 - y^2 \ln y])^{-2}\, e^{9.836(\frac{5}{6} - \frac{1}{3}\ln y)/\emptyset^{1/2}} \quad . \tag{6}$$

For a sharp emitter with a hemispherical tip of radius *r*, $\beta = 1/(5\mathrm{r})$ empirically and its value is $\beta = 1.3 \times 10^7/\mathrm{m}$ [37-38]. Substitute the β value to equation (2), the turn-on field and threshold field are obtained as 2.7 V/nm at 2 nA and 3.5 V/nm at 50 nA, respectively. The measured slope *k* = –2762 and the work function are obtained as 3.2 eV, which is slightly lower than the work function measured at the (100) surface of bulk HfC crystal [18]. It is also in agreement with the value deduced from HfC nanowire sharpened by FIB method[14].

Emission stability is of crucial importance for the point electron source. Figure 3a is the stability of the emission current at 53 nA measured for 30 min in a vacuum of 3×10^{-7} Pa. The fluctuation is calculated by $< \Delta I^2 >^{1/2}/< I >$ (in which $< I >$ is the average current and $\Delta I = I - < I >$ is the deviation of current from its average value) and the value is 1.4%. In addition, it has no noticeable decay in emission current within the duration 30 min, which is a significant improvement compared with the W(310) CFE electron source. When the emission time is extended, step noises appeared which were attributed to gas adsorption and desorption due to the lower vacuum and they could be eliminated by thermal flashing. It was also shown that, when the nanoneedle emitter was operated in a same high vacuum (10^{-9} Pa) as W(310) CFE point electron source, the step noises were removed and the a stable long-term emission with a fluctuation smaller than 1% in 100 hours without flashing could be achieved [31].

A higher emission current results in a higher beam brightness, which is highly demand for enhancing the signal-to-noise ratio of images. Figure 3b-c show that the fluctuations in emission current of 148 nA and 279 nA in 15 min are 0.8% and 1.5%, respectively. For comparison, the fluctuation in emission current of 53 nA in 15 mins is 0.7%. Although the higher emission current causes

slightly larger fluctuation due to the larger emission area and also more chances to induce ion ionization and bombardment, the HfC emitter still exhibited an excellent stability and smaller fluctuations that the contemporary W(310) CFE electron source. In addition, no deterioration in high current was observed. These results show that the HfC nanoneedle emitter has the capability to deliver a stable emission of high current.

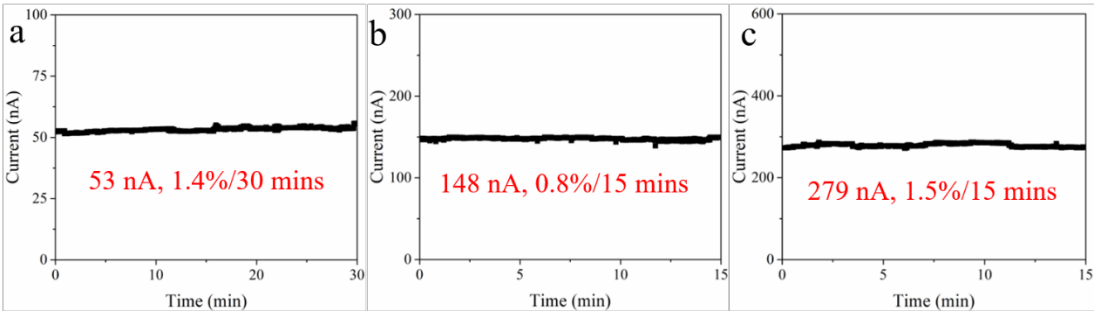

Figure 3 Emission stability under different current and duration. (a) 53 nA, fluctuation of 1.4%/30 min; (b) 148 nA, fluctuation of 0.8%/15 min; (c) 279 nA, fluctuation of 1.5%/15 min.

Conclusions

HfC field-emission point electron source can now be fabricated into a robust structure of nanoneedle morphology by using controllable FIB techniques. The HfC nanoneedle emitter has a very sharp tip and it retains its single-crystalline structure as shown by transmission electron microscopy and energy-dispersive spectroscopy characterizations. The HfC nanoneedle emitter can deliver an electron beam of low divergence, low turn-on voltage. Of particular importance of the HfC nanoneedle field-emitter is that it can offer field emission of high stability even under a high current of ~300 nA. The low work function, high emission current, and high emission stability make HfC nanoneedle an excellent candidate for high-performance point electron sources.

Methods

***Fabrication of HfC nanoneedle emitter*:** The HfC nanoneedle emitter was fabricated

from a (100) oriented HfC crystal by a lift-out method using a FIB-SEM dual beam system (FEI Helios 650). The fabrication processes include: (i) A W(310) needle with radius of 100 nm was processed by FIB to produce a flat platform at its tip; (ii) A piece of HfC was lift-out from the HfC crystal bulk and transferred onto the flat platform of W(310) needle; (iii) Apply FIB milling to sharpen the HfC tip with Ga-ion beam to obtain the designed structure and geometry.

Structural characterization: The HfC nanoneedle was transferred on a TEM grid using a FIB-SEM system. The microstructure and chemical composition of the HfC nanoneedle were characterized by both TEM and Cs-corrected scanning transmission electron microscopy (FEI Titan 80-200 kV) equipped with an energy-dispersive X-ray spectrometer (EDS).

***Measurement of field-emission*:** The field-emission characteristics were measured in a high vacuum chamber of base pressure 3×10^{-7} Pa. In the high vacuum chamber, a negative voltage was applied on the HfC nanoneedle emitter to induce electron emission. A grounded annular extractor with a diameter of 1 cm was placed in front of HfC nanoneedle emitter. A grounded microchannel plate (MCP) was placed in front of the HfC nanoneedle emitter to observe the field emission pattern. The distance between the HfC emitter and MCP was about 5 cm. An electrometer (Keithley 6514) was connected between the power supply and emitter for measurement of the total emission current.

Credit author statement

Shuai Tang: Methodology, Validation, Formal analysis, Investigation, Visualization, Writing – original draft, Writing – review & editing. **Jie Tang:** Conceptualization, Supervision, Funding acquisition, Writing – original draft, Writing – review & editing. **Yimeng Wu:** Formal analysis, Writing – review & editing. **You-Hu Jun:** Formal analysis, Writing – review & editing. **Jun Uzuhashi:** Investigation, Writing – review & editing. **Tadakatsu Ohkubo:** Investigation, Writing – review & editing. **Masaki**

Takeguchi: Formal analysis, Writing – review & editing. **Lu-Chang Qin:** Conceptualization, Writing – original draft, Writing – review & editing.

Declaration of competing interest

The authors declare that they have no known competing financial interests or personal relationships that could have appeared to influence the work reported in this paper.

Data and materials availability

The data that support the findings of this study are available from the corresponding authors upon reasonable request.

Acknowledgement

A part of this work was also supported by the Nanostructural Characterization Group of the NIMS Electron Microscopy Analysis Station.

References

1 G. Schwind, G. Magera, L. Swanson, Comparison of parameters for Schottky and cold field emission sources, J. Vac. Sci. Technol. B 24 (2006) 2897-2901.

2 Y. Kohno, E. Okunishi, T. Tomita, I. Ishikawa, T. Kaneyama, Y. Ohkura, Y. Kondo, T. Isabell, Development of a cold field-emission gun for a 200kV atomic resolution electron microscope, Microsc. Anal. 24 (2010) S9-13.

3 H. Sawada, N. Shimura, K. Satoh, E. Okunishi, S. Morishita, T. Sasaki, Y. Jimbo, Y. Kohno, F. Hosokawa, T. Naruse, M. Hamochi, T. Sato, K. Terasaki, T. Suzuki, M. Terao, S. Waki, T. Nakamichi, A. Takano, Y. Kondo, T. Kaneyama, Super high resolution imaging with atomic resolution electron microscope of JEM-ARM300F, JEOL News 49 (2014) 51-58.

4 K. Kasuya, S. Katagiri, T. Ohshima, S. Kokubo, Stabilization of a tungsten <310> cold field emitter, J. Vac. Sci. Technol. B 28 (2010) L55-L60.

5 L. W. Swanson, L. C. Crouser, Total-energy distribution of field-emitted electrons and single-plane work functions for tungsten, Phys. Rev. 163 (1967) 622.

6 W. A. de Heer, A. Chatelain, D. Ugarte, A carbon nanotube field-emission electron source, Science 270 (1995) 1179-1180.

7 Y. Saito, K. Hamaguchi, K. Hata, K. Uchida, Y. Tasaka, F. Ikazaki, M. Yumura, A. Kasuya, Y. Nishina, Conical beams from open nanotubes, Nature 389 (1997) 554-555.

8 N. de Jonge, Y. Lamy, K. Schoots, T. Oosterkamp, High brightness electron beam from a multi-walled carbon nanotube, Nature 420 (2002) 393-395.

9 G. Zhao, J. Zhang, Q. Zhang, H. Zhang, O. Zhou, L.-C. Qin, J. Tang, Fabrication and characterization of single carbon nanotube emitters as point electron sources, Appl. Phys. Lett. 89 (2006) 193113.

10 S. Tang, Y. Zhang, P. Zhao, R. Z. Zhan, J. Chen, S. Z. Deng, Realizing the large current field emission characteristics of single vertical few-layer graphene by constructing a lateral graphite heat dissipation interface, Nanoscale 13 (2021) 5234-5242.

11 X. Shao, A. Srinivasan, W. K. Ang, A. Khursheed, A high-brightness large-diameter graphene coated point cathode field emission electron source, Nat. Comm. 9 (2018) 1-8.

12 J. S. Yuan, H. Zhang, J. Tang, N. Shinya, K. Nakajima, L.-C. Qin, Field emission from single-crystalline HfC nanowires, Appl. Phys. Lett. 100 (2012) 113111.

13 S. Tang, J. Tang, T.-W. Chui, W. Hayami, J. Uzuhashi, T. Ohkubo, F. Uesugi, M. Takeguchi, M. Mitome, L.-C. Qin, A HfC nanowire point electron source with oxycarbide surface of lower work function for high-brightness and stable field-emission, Nano Res. 13 (2020) 1620-1626.

14 S. Tang, J. Tang, T. Chui, J. Uzuhashi, D. Tang, T. Ohkubo, M. Mitome, F. Uesugi, M. Takeguchi, L.-C. Qin, A controllable and efficient method for the fabrication of a single HfC nanowire field-emission point electron source aided by low keV FIB milling, Nanoscale 12 (2020) 16770-16774.

15 T.-W. Chiu, J. Tang, S. Tang, J. Yuan, L.-C. Qin, Synthesis and field emission of ZrC nanowire, Mater. Today Comm. 25 (2020) 101240.

16 T.-W. Chiu, J. Tang, S. Tang, W. Hayami, J. Yuan, L.-C. Qin, Reduced work function and improved field emission stability of ZrC nanowires upon surface oxidation, Appl. Phys. Lett. 117 (2020) 053101.

17 H. Zhang, J. Tang, J. Yuan, Y. Yamauchi, T. T. Suzuki, N. Shinya, K. Nakajima, L.-C. Qin, An ultrabright and monochromatic electron point source made of a LaB_6 nanowire, Nat. Nanotechnol. 11 (2016) 273-280.

18 W. A. Mackie, J. L. Morrissey, C. H. Hinrichs, P. R. Davis, Field emission from hafnium carbide, J. Vac. Sci. Technol. A 10 (1992) 2852-2856.

19 M. Yu, B. Hussey, E. Kratschmer, T. Chang, Improved emission stability of carburized HfC< 100> and ultrasharp tungsten field emitters, J. Vac. Sci. Tech. B 13 (1995) 2436-2440.

20 K. J. Kagarice,. G. Magera, S. D. Pollard, W. A. Mackie, Cold field emission from HfC(310), J. Vac. Sci. Technol. B 26 (2008) 868-871.

21 G. Singh, R. Bücker, G. Kassier, M. Barthelmess, F. S. Zheng, V. Migunov, M. Kruth, R. E. Dunin-Borkowski, S. T. Purcell, R. J. Dwayne Miller, Fabrication and characterization of a focused ion beam milled lanthanum hexaboride based cold field electron emitter source, Appl. Phys. Lett. 113 (2018) 093101.

22 K. Kasuya, T. Kusunoki, T. Hashizume, T. Ohshima, S. Katagiri, Y. Sakai, N. Arai, Appl. Phys. Lett. 117 (2020) 213103.

23 R. Andrievskii, N. Strel'nikova, N. Poltoratskii, E. Kharkhardin, V. Smirnov, Melting point in systems ZrC-HfC, TaC-ZrC, TaC-HfC, Powder Metall. Met. C 6 (1967) 65-67.

24 W. Williams, Electrical properties of hard materials, Int. J. Refract. Met. H. 17 (1999) 21-26.

25 M. Opeka, I. Talmy, E. Wuchina, J. Zaykoski, S. Causey, Mechanical, thermal, and oxidation properties of refractory hafnium and zirconium compounds, J. Eur. Ceram. Soc. 19 (1999) 2405-2414.

26 M. R. Rakhshandehroo, S. W. Pang, High current density Si field emission devices with plasma passivation and HfC coating, IEEE T. Electron Dev. 46 (1999) 792-797.

27 J. H. Zhang, C. R. Yang, Y. J. Wang, T. Feng, W. D. Yu, J. Jiang, X. Wang, X. H. Liu, Improvement of the field emission of carbon nanotubes by hafnium coating and annealing, Nanotechnology 17 (2005) 257.

28 Y. C. Yang, L. Liu, Y. Wei, P. Liu, K. L. Jiang, Q. Q. Li, S. S. Fan, In situ fabrication of HfC-decorated carbon nanotube yarns and their field-emission properties, Carbon 48 (2010) 531-537.

29 S. Tang, J. Tang, J. Uzuhashi, T. Ohkubo, W. Hayami, J. S. Yuan, M. Takeguchi, M. Mitome, L.-C. Qin, A stable LaB_6 nanoneedle field-emission point electron source, Nanoscale Adv. 3 (2021) 2787-2792.

30 S. Tang, J. Tang, Y. M. Wu, Y.-H. Chen, J. Uzuhashi, T. Ohkubo, L.-C. Qin, Stable field-emission from a CeB_6 nanoneedle point electron source, Nanoscale 13 (2021) 17156-17161.

31 S. Tang, J. Tang, E. Okunishi, Y. Ninota A. Yasuhara, J. Uzuhashi, T. Ohkubo, M. Takeguchi, J. S. Yuan, L.-C. Qin, A stable LaB_6 nanoneedle field-emission

electron source for atomic resolution imaging with a transmission electron microscope, Mater. Today 57 (2022) 35-42.

32 C. Oshima, E. Bannai, T. Tanaka, S. Kawai, Thermionic work function of LaB_6 single crystals and their surfaces, J. Appl. Phys. 48 (1977) 3925-3927.

33 E. L. Murphy, R. H. Good Jr, Thermionic emission, field emission, and the transition region, Phys. Rev. 102 (1956) 1464.

34 R. G. Forbes, Simple good approximations for the special elliptic functions in standard Fowler-Nordheim tunneling theory for a Schottky-Nordheim barrier, Appl. Phys. Lett. 89 (2006) 113122.

35 R. G. Forbes, J. H. B. Deane, Reformulation of the standard theory of Fowler–Nordheim tunnelling and cold field electron emission, Proc. Roy. Soc. A- Math. Phys. 463 (2007) 2907-2927.

36 R. G. Forbes, Comment on "Advanced field emission measurement techniques for research on modern cold cathode materials and their applications for transmission-type x-ray sources", Rev. Sci. Instrum. 91 (2020) 107101.

37 R. Gomer, Field Emission and Field Ionization, 2nd Ed., (Harvard University Press: 1961).

38 Y. Saito, S. Uemura, Field emission from carbon nanotubes and its application to electron sources, Carbon 38 (2020) 169-182.